iScience

CellPress
OPEN ACCESS

Article

Chronic cold exposure induces autophagy to promote fatty acid oxidation, mitochondrial turnover, and thermogenesis in brown adipose tissue

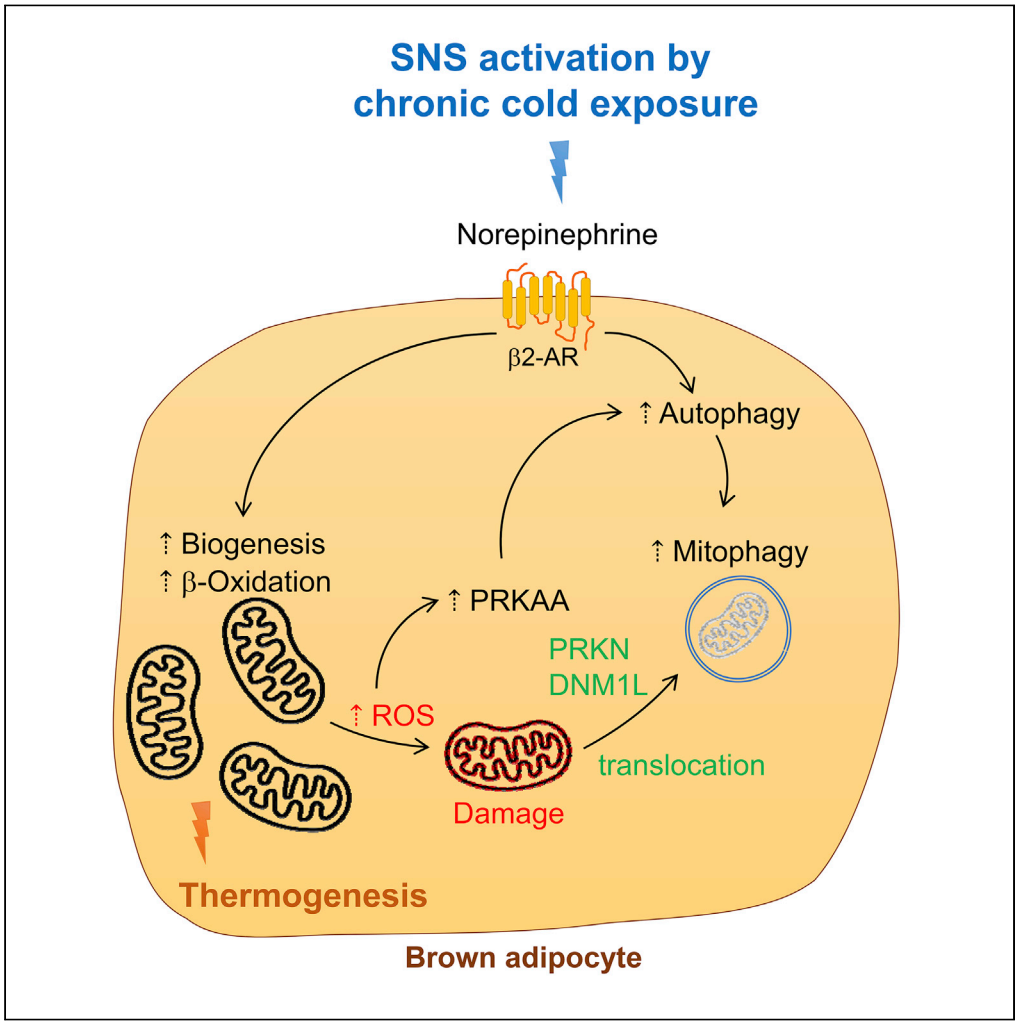

Winifred W. Yau, Kiraely Adam Wong, Jin Zhou, ..., Boon-Huat Bay, Brijesh Kumar Singh, Paul Michael Yen

paul.yen@duke-nus.edu.sg

Highlights

Chronic cold stress stimulates β-oxidation in BAT to increase thermogenesis

Chronic cold stress stimulates mitophagy in BAT

Autophagy is critical for mitochondrial quality control to sustain thermogenesis

Yau et al., iScience *24*, 102434
May 21, 2021 © 2021
https://doi.org/10.1016/j.isci.2021.102434

iScience

CellPress
OPEN ACCESS

Article

Chronic cold exposure induces autophagy to promote fatty acid oxidation, mitochondrial turnover, and thermogenesis in brown adipose tissue

Winifred W. Yau,[1] Kiraely Adam Wong,[1] Jin Zhou,[1] Nivetha Kanakaram Thimmukonda,[1] Yajun Wu,[2] Boon-Huat Bay,[2] Brijesh Kumar Singh,[1] and Paul Michael Yen[1,3,4,*]

SUMMARY

Autophagy plays an important role in lipid breakdown, mitochondrial turnover, and mitochondrial function during brown adipose tissue (BAT) activation by thyroid hormone, but its role in BAT during adaptive thermogenesis remains controversial. Here, we examined BAT from mice exposed to 72 h of cold challenge as well as primary brown adipocytes treated with norepinephrine and found increased autophagy as well as increased β-oxidation, mitophagy, mitochondrial turnover, and mitochondrial activity. To further understand the role of autophagy of BAT *in vivo*, we generated BAT-specific *Atg5* knockout (*Atg5*cKO) mice and exposed them to cold for 72 h. Interestingly, BAT-specific *Atg5*cKO mice were unable to maintain body temperature after chronic cold exposure and displayed deranged mitochondrial morphology and reactive oxygen species damage in their BAT. Our findings demonstrate the critical role of autophagy in adaptive thermogenesis, fatty acid metabolism, and mitochondrial function in BAT during chronic cold exposure.

INTRODUCTION

Adaptive thermogenesis is an essential survival mechanism for homeotherms that occurs whenever the ambient temperature falls below thermoneutrality (Silva, 2003). Brown adipose tissue (BAT) is a specialized tissue for generating adaptive thermogenesis (Lowell and Spiegelman, 2000; Stock, 1989) with high oxidative capacity. During sustained cold exposure, BAT undergoes remodeling to increase its thermogenic potential. Chronic cold exposure causes increased mitochondrial activity in BAT with induction of β-oxidation of fatty acids, electron transport activity, and uncoupling protein 1 (UCP1) expression to generate heat (Cannon and Nedergaard, 2004; Blondin et al., 2014, 2017). However, this increased mitochondrial activity also increases reactive oxygen species (ROS) (Barja De Quiroga et al., 1991; Buzadzic et al., 1999) that can lead to mitochondrial damage and impaired thermogenesis (Lettieri-Barbato, 2019).

To prevent accumulation of oxidative damage, BAT utilizes autophagy to remove and recycle damaged organelles such as mitochondria (mitophagy). BAT-specific knockdown of autophagy led to mitochondrial damage in BAT and impaired thermogenesis by thyroid hormone (T_3) (Yau et al., 2019). However, the role of autophagy in BAT during cold exposure is not well understood as there are conflicting results in the literature (Martinez-Lopez et al., 2016) (Cairo et al., 2016; Lu et al., 2018). Martinez-Lopez et al. found that lipophagy was acutely upregulated after 1-h cold exposure to facilitate lipid utilization (Martinez-Lopez et al., 2016). Cairo et al. showed that autophagy was inhibited after 24 h of cold exposure and was associated with reduced clearance of UCP1 to facilitate heat generation (Cairo et al., 2016). On the other hand, Lu et al. observed increased mitophagy after 7 days of cold exposure (Lu et al., 2018). To better understand the regulation of autophagy during adaptive thermogenesis and autophagy's role in lipid metabolism and mitochondrial activity in BAT during cold stress, we examined autophagy in BAT from mice exposed to chronic cold exposure for 72 h and in primary brown adipocytes treated with norepinephrine (NE). Autophagy in BAT was highly stimulated after chronic cold exposure and in brown adipocytes after NE stimulation. This induction of autophagy was accompanied by increased autophagy gene transcription, β-oxidation of fatty acids, mitophagy, and mitochondrial turnover. BAT-specific *Atg5* KO mice also were unable to maintain body temperature during cold exposure and showed evidence of ROS damage in BAT. Our findings demonstrate the critical role of autophagy for thermogenesis in BAT during chronic cold exposure and its impact on lipid metabolism and mitochondrial function.

[1]Laboratory of Hormonal Regulation, Cardiovascular and Metabolic Disorders Program, Duke NUS Medical School, Singapore 169857, Singapore

[2]Department of Anatomy, Yong Loo Lin School of Medicine, National University of Singapore, Singapore 117594, Singapore

[3]Duke Molecular Physiology Institute, Duke University, Durham, NC 27708, USA

[4]Lead contact

*Correspondence: paul.yen@duke-nus.edu.sg

https://doi.org/10.1016/j.isci.2021.102434

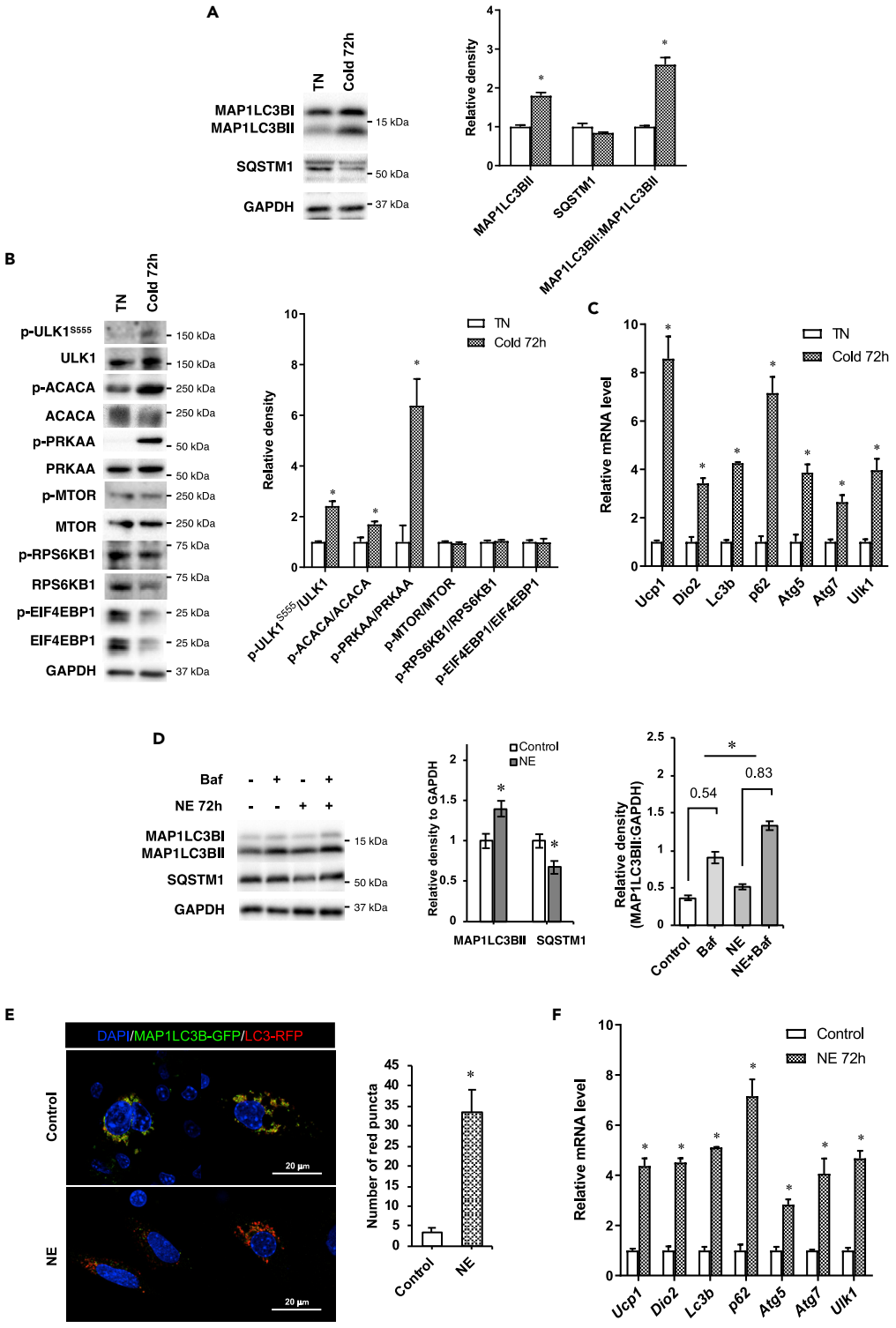

Figure 1. Chronic cold exposure increases autophagy in BAT and primary brown adipocytes

(A) Representative immunoblots and densitometry analysis of MAP1LC3BII, SQSTM1, and MAP1LC3BII:MAP1LC3BI ratio in BAT of mice subjected to 72 h of cold exposure.

(B) Immunoblots and densitometry analysis of PRKAA and MTOR pathway in BAT during cold exposure.

(C) mRNA expression of autophagy genes in the BAT of mice exposed to cold. Values are means ± SEM for 5 mice in each group.

Figure 1. *Continued*

(D) Autophagy flux analysis in primary brown adipocytes. Cells were treated with or without NE for 72 h, and bafilomycin (Baf) was added 6 h before harvest.

(E) Confocal microscopic images and quantification of red puncta in brown adipocyte cell line transfected with RFP-eGFP-MAP1LC3B plasmid and incubated with or without 1 μM NE for 72 h. Scale bar, 20 μm. Quantification of images (at least 10 transfected cells per sample in 3 different fields) was done using ImageJ software.

(F) mRNA expression of autophagy genes in primary brown adipocytes treated with 1 μM NE for 72 h. Statistical significance shows as *$p < 0.05$.

RESULTS

Chronic cold challenge induces autophagy in BAT

To examine the effect of cold exposure on autophagy in BAT, we housed C57BL/6J mice at 4°C for 72 h and at 30°C, the thermoneutral (TN) temperature for mice. Mice then were sacrificed and BAT harvested for analyses. After 72 h of cold exposure, there was a marked increase in MAP1LC3BII/microtubule-associated protein 1 light chain 3 beta II and decrease in SQSTM1 protein expression as well as increased MAP1LC3BI to MAP1LC3BII conversion suggesting there was an increase in autophagy after chronic cold exposure (Figure 1A).

PRKAA/AMPK activation stimulates autophagy by phosphorylating the autophagosome initiator protein, Unc-51 Like Autophagy Activating Kinase 1 (ULK1) at serine 555 (S555) (Egan et al., 2011; Mao and Klionsky, 2011). In contrast, MTOR activation inhibits autophagy (Kim and Guan, 2015). We observed an increase in phosphorylation of PRKAA, its downstream target ACC, as well as ULK1 at S555 but no change in phosphorylation of MTOR or its downstream targets RPS6KB1 and EIF4EBP1, demonstrating that PRKAA was driving the increase in autophagy (Figure 1B). At the transcriptional level, there was induction of *Map1lc3b*, *Sqstm1*, *Atg5*, *Atg7*, and *Ulk1* mRNA levels at 72 h suggesting that the increase in autophagy was associated with an increase in autophagy gene expression at 72 h (Figure 1C). Consistent with BAT activation, the mRNA levels of *Ucp1* and *Dio2* were also up-regulated after 72 h of cold exposure (Figure 1C).

Long-term NE treatment induces autophagy in primary brown adipocytes

Cold exposure activates adrenergic signaling in BAT to initiate thermogenesis (Silva, 2003). We next examined the direct effect of adrenergic stimulation on BAT autophagy by treating primary brown adipocytes with NE. We observed that when cells were treated with NE for 72 h, they showed increased MAP1LC3BII and reduced SQSTM1 expression that was consistent with increased autophagy flux (Figure 1D). When we used bafilomycin (Baf), to block late autophagy, there was a greater increase in MAP1LC3BII after Baf addition in the NE-treated cells versus untreated control cells (0.83 versus 0.54), showing that NE increased autophagic flux (Figure 1D). We further examined autophagic flux by transfecting a tandem fluorescent *Map1lc3b* (RFP-eGFP-MAP1LC3B) plasmid expressing MAP1LC3B with the green and red fluorescent domains into a brown adipocyte mouse mBAP-9 cell line. Both green and red signals are emitted when the fusion protein is within an autophagosome. However, the green signal is quenched and only red fluorescence is emitted in the acidic environment of the fused autolysosome. In cells incubated with NE for a period of 72 h, there was increased number of red puncta indicating they had higher autophagic flux than control cells (Figure 1E).

Similar to our *in vivo* observations after cold exposure, we observed induction of autophagy gene expression after 72 h of NE treatment in primary brown adipocytes (Figure 1F). We also detected upregulation of *Ucp1* and *Dio2* gene expression after 72 h of NE treatment. These results strongly suggested that autophagy was activated after chronic BAT stimulation.

Chronic cold exposure increases β-oxidation of fatty acids in BAT

To examine mitochondrial activity in BAT after chronic cold exposure, we next performed analyses of acylcarnitine and tricarboxylic acid (TCA) intermediates in BAT from mice exposed to cold temperature for 72 h. Chronic cold exposure significantly increased short-, medium-, and long-chain acylcarnitine species (Figures 2A–2C) suggesting there was increased mitochondrial β-oxidation. The level of acetyl-CoA (C2 carnitine) was only mildly upregulated, most likely due to rapid oxidation of acetyl-CoA via the TCA cycle because TCA cycle intermediates also were increased (Figure 2D). Additionally, we found that phosphorylated adipose triglyceride lipase (PNPLA2/ATGL) and hormone-sensitive lipase (LIPE/HSL) were both decreased, whereas CPT1α and MCAD1 protein expression were increased (Figure 2E). These findings highlighted that autophagy, rather than lipase activity, may be the major mechanism for mobilizing triglycerides from fat droplets and hydrolyzing them to free fatty acids for mitochondrial β-oxidation. Taken

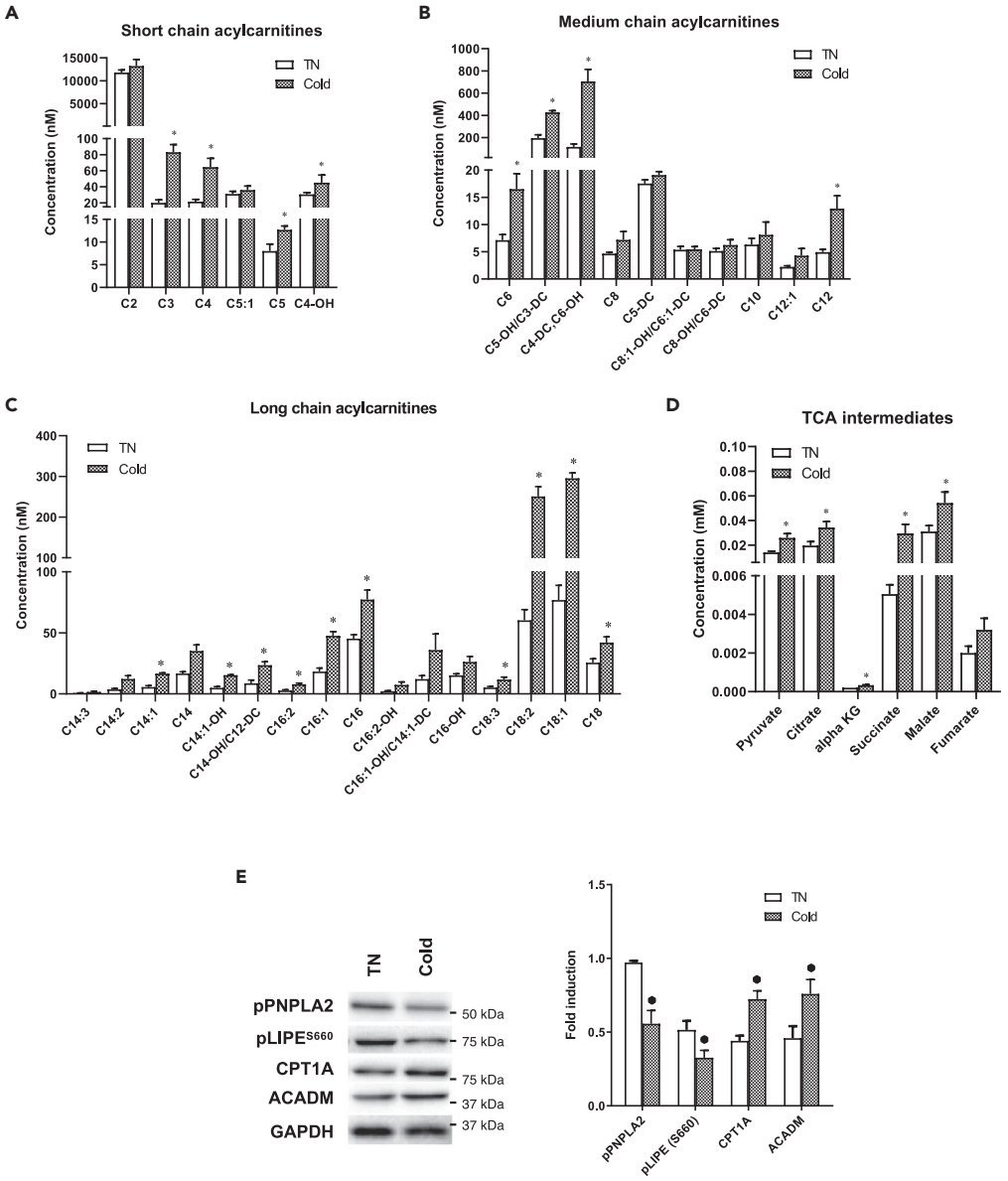

Figure 2. Chronic cold exposure induces lipophagy and β-oxidation in BAT

(A–D) Metabolomic profiling of (A) short-, (B) medium-, and (C) long-chain acylcarnitines species and (D) level of TCA cycle intermediates in BAT.

(E) Immunoblot and densitometry analysis of lipases and β-oxidation markers in BAT. Values are means ± SEM for 5 mice in each group. Statistical significance shows as *p < 0.05.

together, these results showed that chronic cold exposure stimulated CPT1α and MCAD protein expression in BAT to increase fatty acid β-oxidation *in vivo*.

Chronic cold exposure increases mitophagy and mitochondrial turnover in BAT

We also examined mitophagy in BAT from mice after 72 h of cold exposure and observed increased amounts of autophagosomes, some of which contained mitochondrial remnants by electron microscopy (Figure 3A). We then analyzed the mitochondrial fraction of BAT and found that both MAP1LC3BII and SQSTM1 proteins were recruited to the mitochondrial fraction of cold-treated mice (Figure 3B). PRKN/E3 ubiquitin-protein ligase parkin and PINK1/PTEN-induced kinase 1 coordinate to activate selective

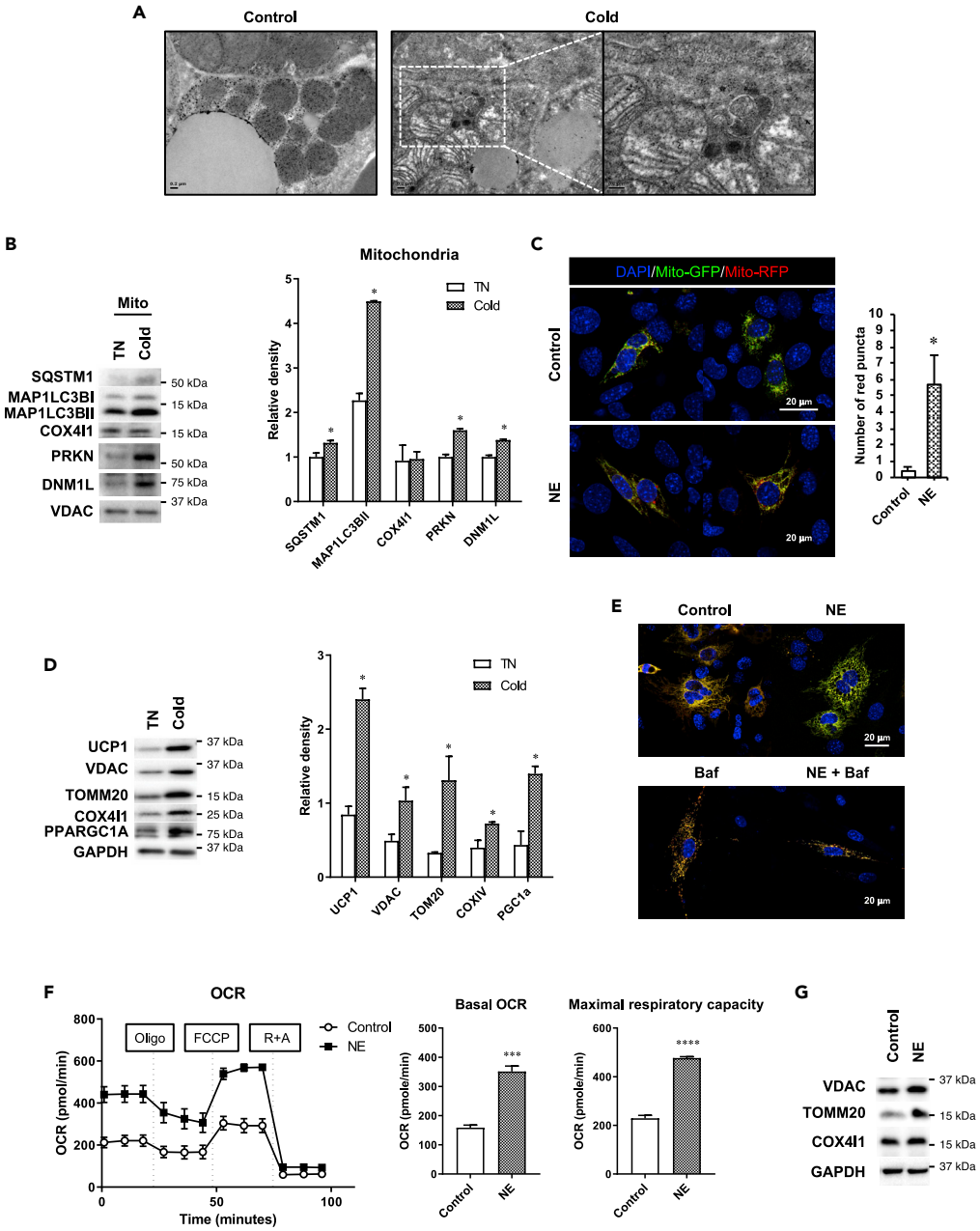

Figure 3. Chronic cold exposure induces mitophagy and mitochondrial turnover in BAT

(A) Representative electron microscopic images showing BAT of mice housed at TN (30°C) or in cold (4°C) for 72 h. White box shows an autophagosome containing mitochondria. Scale bar, 0.2 μm.

(B) Immunoblots and densitometry of autophagy proteins in mitochondrial fraction of BAT.

(C) Confocal microscopic images and quantification of red puncta in brown adipocyte cell line transfected with mito-RFP-EGFP plasmid and treated with or without 1 μM NE for 72 h. Scale bar, 20 μm. Quantification of images (at least 10 transfected cells per sample in 3 different fields) was done using ImageJ software.

(D) Immunoblots and densitometry of mitochondrial proteins in BAT.

(E) Confocal microscopic images showing brown adipocyte cell line transfected with pMitoTimer plasmid and treated with or without 1 μM NE for 72 h. Bafilomycin (Baf) was added 6 h before harvest. Scale bar, 20 μm.

(F) Seahorse analysis of oxygen consumption rate (OCR) for primary brown adipocytes treated with 1 μM NE for 72 h. For the NE-treated group, 1 μM NE was added to the assay media 1 h before OCR measurement.

(G) Representative immunoblots and densitometry showing mitochondrial protein expression in primary brown adipocytes treated with 1 μM NE for 72 h. Statistical significance shows as *$p < 0.05$, ***$p < 0.001$ and ****$p < 0.0001$.

mitophagy of damaged mitochondria (Wei et al., 2015; Jin and Youle, 2012; Bingol and Sheng, 2016). Dynamin-related protein 1 (DNM1L/DRP1) is responsible for mitochondrial fission, which facilitates PRKN-mediated mitophagy (Burman et al., 2017). Of note, DNM1L and PRKN levels were significantly higher in the mitochondrial fraction of BAT from mice exposed to 72 h of cold challenge than those from control mice (Figure 3B) and suggest that mitochondrial fission and mitophagy were increased by chronic cold exposure.

We next transfected mBAP-9 brown adipocytes with a tandem-tagged mito-RFP-EGFP plasmid, which encoded a fusion protein containing a mitochondrial targeting signal with green and red fluorescent proteins, with and without NE for 72 h. Similar to MAP1LC3B-RFP-EGFP, only red fluorescence is detected after mitochondria are localized within autolysosomes (mitophagy). NE treatment markedly increased the number of red puncta (Figure 3C) and demonstrated that β-adrenergic stimulation of brown adipocytes increased mitophagy.

Cold exposure for 72 h significantly increased the expression of mitochondrial proteins such as UCP1, VDAC, TOMM20, and COX4I1 as well as the master regulator for mitochondrial biogenesis, PCG1α (Figure 3D). These findings suggested that there was significant mitochondrial biogenesis that led to an overall net gain of mitochondrial level despite active mitophagy. To further examine mitochondrial turnover, we transfected mBAP-9 cells with a pMitoTimer plasmid (Laker et al., 2014), a fluorescent protein containing a DsRed mutation that causes a time-dependent transition from green fluorescence to a more stable red conformation over 48 h (Terskikh et al., 2000) to monitor the synthesis, maturation, and degradation of mitochondria. In the control cells, we detected both red and green signals, resulting in a yellow color in the overlay (Figure 3E). However, treating cells with NE for 72 h reduced the red signal and increased the green fluorescent signal indicating removal of mature mitochondria and synthesis of new mitochondria under this condition (Figure 3E). Moreover, when autophagy was inhibited by Baf, NE treatment did not reduce the red signal, suggesting that mitochondrial clearance was blocked by decreased mitophagy. Taken together, these findings suggested that there was both degradation of mature mitochondria by mitophagy and synthesis of new mitochondria that led to a net increase in the total amount of mitochondria. We next examined the effect of this increased mitochondrial turnover on mitochondrial respiration by Seahorse oximetry by treating primary brown adipocytes with NE for 72 h. These cells showed significantly higher basal oxygen consumption rate (OCR) as well as maximum respiratory capacity than untreated cells (Figure 3F). Consistent with increased mitochondrial activity, NE-treated cells also showed increased amounts of mitochondrial proteins (Figure 3G). Collectively, these findings showed that β-adrenergic stimulation increased mitophagy, mitochondria number, and mitochondrial turnover to stimulate mitochondrial respiration.

Autophagy is essential for BAT thermogenesis during chronic cold exposure

To determine whether autophagy was absolutely required for thermogenesis during chronic cold challenge, we generated BAT-specific *Atg5* conditional knockout mice (*Atg5*cKO) by injecting *Ucp1* promoter-driven *Cre*-expressing adeno-associated virus (AAV) into $Atg5^{flox/flox}$ mice and exposed them to either TN conditions or cold challenge for 72 h. After harvesting BAT, we confirmed that Atg5 expression was decreased in *Atg5*cKO mice but they did not exhibit any decrease in autophagy at TN (Figure 4A). During chronic cold exposure, BAT from control mice increased expression of Atg5, MAP1LC3BII, and SQSTM1 protein as well as MAP1LC3BII: MAP1LC3BI ratio consistent with high autophagic flux (Figure 4A). In contrast, BAT from *Atg5*cKO mice showed no change in MAP1LC3BII, increased SQSTM1, and reduced MAP1LC3BII:MAP1LC3BI ratio in response to cold exposure, suggesting there was decreased autophagy flux (Figure 4A). When we examined body temperature, wild-type (WT) and *Atg5*cKO mice maintained body temperature at TN and WT mice maintained body temperature after 72-h cold exposure (Figure 4B). In contrast, *Atg5*cKO mice were unable to sustain their body temperature after cold exposure (Figure 4B). These findings clearly demonstrated that autophagy in BAT was necessary for thermogenesis *in vivo* during chronic cold exposure.

We next examined the effects of blocking autophagy in BAT on mitochondria after 72-h cold exposure. Using electron microscopy, we found that BAT mitochondria from WT mice had an elongated oval shape at TN. Upon cold challenge, these mitochondria became more round but maintained intact membranes and normal cristae structure. Interestingly, when *Atg5*cKO mice were exposed to chronic cold challenge, BAT mitochondria became swollen and contained distorted cristae (Figure 4C). Additionally, protein carbonyl

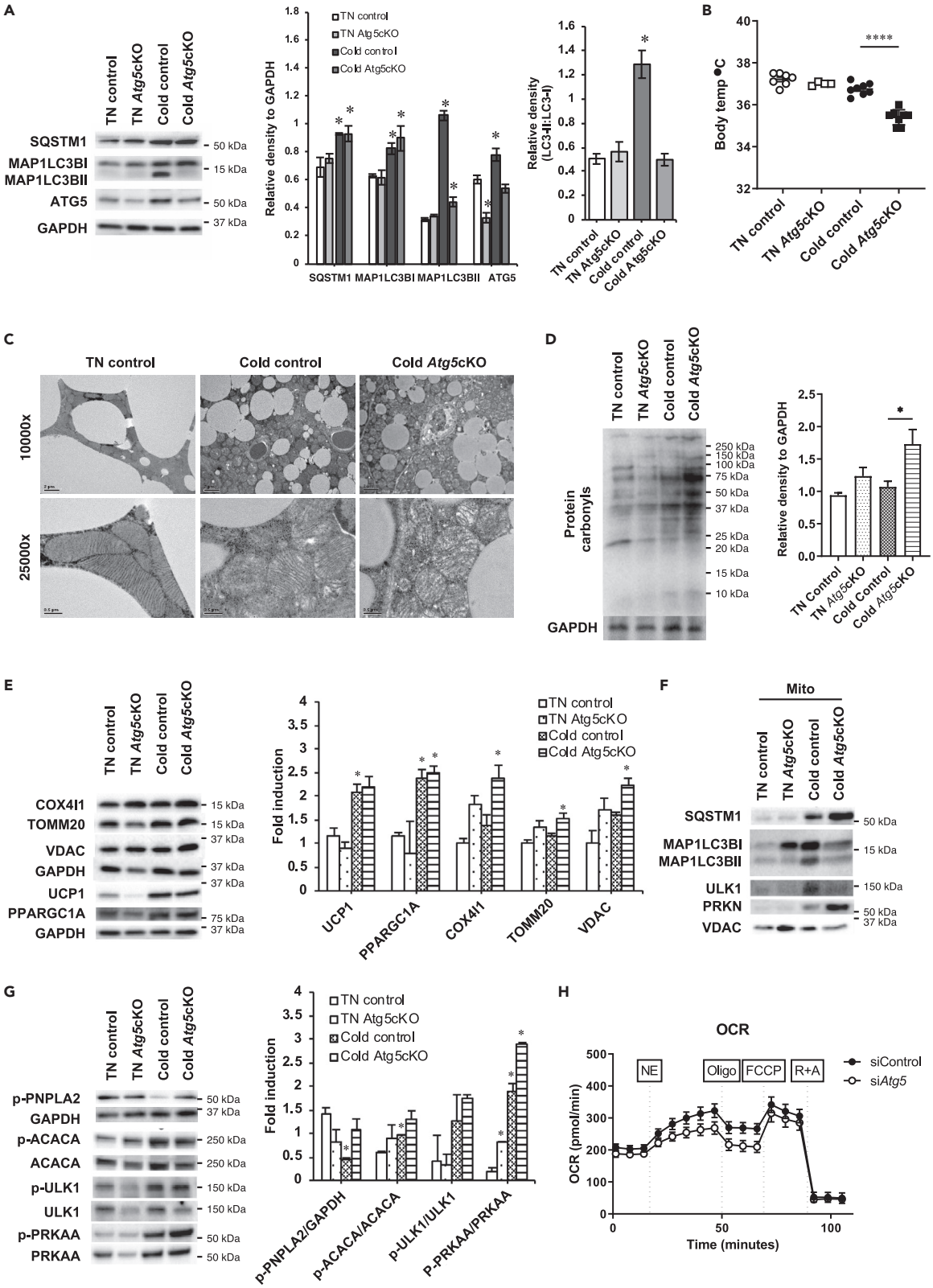
A
TN control
TN Atg5cKO
Cold control
Cold Atg5cKO
SQSTM1
MAP1LC3BI
MAP1LC3BII
ATG5
GAPDH
50 kDa
15 kDa
50 kDa
37 kDa
Relative density to GAPDH
SQSTM1 MAP1LC3BI MAP1LC3BII ATG5
Relative density (LC3-II:LC3-I)
B
Body temp °C
****
C
TN control
Cold control
Cold Atg5cKO
10000x
25000x
D
Protein carbonyls
GAPDH
250 kDa
150 kDa
100 kDa
75 kDa
50 kDa
37 kDa
25 kDa
20 kDa
15 kDa
10 kDa
Relative density to GAPDH
E
COX4I1
TOMM20
VDAC
GAPDH
UCP1
PPARGC1A
GAPDH
Fold induction
UCP1
PPARGC1A
COX4I1
TOMM20
VDAC
F
Mito
SQSTM1
MAP1LC3BI
MAP1LC3BII
ULK1
PRKN
VDAC
G
p-PNPLA2
GAPDH
p-ACACA
ACACA
p-ULK1
ULK1
p-PRKAA
PRKAA
p-PNPLA2/GAPDH
p-ACACA/ACACA
p-ULK1/ULK1
P-PRKAA/PRKAA
H
OCR
NE
Oligo
FCCP
R+A
siControl
siAtg5
OCR (pmol/min)
Time (minutes)

Figure 4. Autophagy in BAT is required for thermogenesis in chronic cold exposure

(A) Representative blots and densitometry of autophagy proteins in BAT of control and *Atg5*cKO mice housed at TN (30°C) or in cold (4°C) for 72 h.

(B) Body temperature of control and *Atg5*cKO mice housed at TN or in cold for 72 h.

(C) Electron microscopic images showing damaged mitochondria in cold-exposed *Atg5*cKO mice. Scale bars: 2 μm (10,000×) and 0.5 μm (25,000×).

(D) Immunoblots and densitometry showing increased level of protein carbonyls in cold-exposed *Atg5*cKO mice.

(E) Representative immunoblots and densitometry showing mitochondrial proteins.

(F) Immunoblots showing autophagy proteins in mitochondrial fraction of BAT.

(G) Representative immunoblots and densitometry of proteins involved in lipolysis and PRKAA pathway in BAT.

(H) Seahorse analysis of OCR in primary brown adipocytes transfected with control or *Atg5* siRNA for 48 h before analysis. Statistical significance shows as *$p < 0.05$ and ****$p < 0.0001$.

See also Figure S1.

formation due to ROS generated from mitochondria was markedly increased in *Atg5*cKO mice during chronic cold exposure but only mildly upregulated in WT mice (Figure 4D). Accordingly, we observed increases of mitochondrial proteins (COX4I1, TOM20, and VDAC but not UCP1) in *Atg5*cKO mice exposed to chronic exposure due to increased accumulation of mitochondria when autophagy was inhibited by *Atg5* KO (Figure 4E). These increases were unlikely due to increased mitochondrial biogenesis after KO because the level of PPARG coactivator 1 alpha (PPARGC1A/PGC1α) protein was not further induced in *Atg5*cKO mice exposed to chronic exposure.

We next analyzed the BAT mitochondrial fractions from WT and *Atg5*cKO mice exposed to chronic cold challenge (Figure 4F). We observed decreased ULK1 accumulation in BAT mitochondria from *Atg5*cKO mice, which in turn led to less MAP1LC3BII recruitment to BAT mitochondria than WT mice. There also was increased PRKN recruitment due to increased mitochondrial membrane damage and decreased mitophagy. Additionally, there was increased SQSTM1 with decreased LC3B recruitment indicative of decreased mitophagy. This decrease in mitophagy most likely led to the morphological changes observed in mitochondria, ROS damage, and insufficient thermogenesis observed in the BAT from *Atg5*cKO mice (Figures 4A–4D).

We next examined the effects of chronic cold exposure on the cell signaling of BAT from *Atg5*cKO mice by measuring phosphorylation of proteins (PNPLA2 and ACACA) involved in lipid metabolism in BAT (Figure 4G). PNPLA2 protein phosphorylation was higher in *Atg5*cKO mice than control mice during cold exposure, suggesting there was a compensatory increase in lipase activity when lipophagy was inhibited. Of note, the BAT expression of *Ucp1* mRNA as well as *sqstm1*, *Map1lc3b*, *Pink1*, and *Prkn* were similar in WT and *Atg5*cKO mice after chronic cold exposure (Figure S1). Phosphorylated PRKAA protein was increased in both WT and *Atg5*cKO mice during chronic cold exposure; however, it was higher in *Atg5*cKO mice (Figure 4E), and was most likely due to lower intracellular ATP, and higher AMP, levels in the *Atg5*cKO mice owing to impaired mitochondrial function (Hinchy et al., 2018). These data were also consistent with the higher ROS damage found in *Atg5*cKO mice because mitochondrial ROS can directly promote PRKAA activation (Rabinovitch et al., 2017). Significantly, the increase in PRKAA did not further increase phosphorylation of ACACA and ULK1, two PRKAA targets, suggesting that inhibition of fatty acid synthesis and ULK1 activation already was maximal in both groups of mice.

Finally, to investigate the effect of autophagy loss on mitochondrial function during chronic cold exposure, we used Seahorse oximetry to measure OCR in primary brown adipocytes transfected with *Atg5* small interfering RNA (siRNA) in the presence of NE (Figure 4G). We found that primary brown adipocytes with *Atg5* knockdown showed significantly less basal OCR, maximal respiratory capacity, and acute NE-stimulated OCR (Figure S1B) than control cells despite having higher amounts of mitochondrial proteins (Figure S1C). These data strongly suggested that impaired autophagy in brown adipocytes led to mitochondrial dysfunction and impaired thermogenic response to NE.

DISCUSSION

In the present study, we report that BAT thermogenesis in response to chronic cold exposure required autophagy. This finding was consistent with earlier reports suggesting there was increased autophagy during long-term cold exposure (Martinez-Lopez et al., 2016; Lu et al., 2018). However, it contrasted with an earlier report of decreased autophagy in BAT after 24 h of cold exposure (Cairo et al., 2016). It is possible that these differences may be due to temporal effects of cold exposure on autophagy, with the increase in autophagy during chronic exposure attributable to the transcriptional induction of autophagy genes that

we observed after 72 h of cold exposure (Figures 1C and 1E). Our findings also were consistent with our previous study showing that T_3 induced autophagy in BAT during activated thermogenesis at room temperature (Yau et al., 2019). Taken together with our findings, induction of autophagy appears to occur during both chronic cold exposure and pharmacological stimulation of BAT.

BAT has been reported to undergo metabolic adaptations such as lipogenesis (Christoffolete et al., 2004), mitochondrial biogenesis (Murholm et al., 2009; Yu et al., 2015; Gospodarska et al., 2015), mitophagy (Lu et al., 2018), and UCP-1 induction during chronic cold exposure. Here, we found that chronic cold stress led to increased fatty acid β-oxidation, mitochondrial turnover, respiration, and thermogenesis in addition to autophagy. We found that chronic cold stress also mildly increased the level of protein carbonyls (Figure 4D) indicative of increased ROS generated by active mitochondria. This increased protein oxidation coincided with the marked increase in mitochondrial activity that occurs in BAT during cold exposure. As ROS directly activates PRKAA (Rabinovitch et al., 2017), it likely plays an important role in stimulating autophagy in BAT during chronic cold exposure to promote mitophagy. We also observed PRKAA activation during chronic cold exposure, which can stimulate autophagy as well as increase transcription of autophagy genes (Sukumaran et al., 2020). This increase in transcription would lead to the synthesis and replenishment of autophagy proteins that are necessary for sustained induction of autophagy.

We found that induction of autophagy/mitophagy was important for removal of damaged mitochondria in BAT after chronic cold exposure or in primary brown adipocytes after NE stimulation (Figures 3C and 3E). These processes were accompanied by recruitment of PRKN and DNM1L protein to BAT mitochondria after chronic cold exposure (Figure 3D). These proteins are critical for mitophagy and mitochondrial fission, respectively. There also was increased mitochondrial turnover, mitochondrial biogenesis, total mitochondrial protein, and mitochondrial activity after cold exposure or NE stimulation (Figures 3C–3F). When autophagy was blocked by inhibiting *Atg5* expression in BAT during cold exposure or NE stimulation of brown adipocytes, both mitochondrial integrity and activity were compromised and were accompanied by a corresponding increase in protein carbonyls reflecting oxidative damage (Figures 4B, 4C, 4D, and 4H). There also was accumulation of PRKN and SQSTM1, and decreased recruitment of ULK1 and MAP1LC3BII in the mitochondrial fraction of BAT, consistent with impaired mitophagy after *Atg*5 KO. Additionally, autophagy per se did not appear to affect mitochondrial biogenesis directly because we observed similar levels of PPARGC1A protein in both control and *Atg5*cKO mice after 72 h of cold exposure. Therefore, it is unlikely that the defective thermogenesis in *Atg5*cKO mice was due to reduced synthesis of healthy mitochondria in BAT. Instead, it is more likely that accumulation of damaged mitochondria from impaired mitophagy increased oxidative stress and damage, which in turn further reduced mitochondrial function. It was reported that mice that lacked all thermogenic capacity, such as the Ucp1 KO mice, had severely reduced body temperature of ~30°C after 3 h of cold (4°C) exposure (Shabalina et al., 2010; Meyer et al., 2010). Interestingly, the *Atg5*cKO mice still were able to maintain their body temperature at ~35.5°C after 72 h of cold exposure suggesting that they still possessed some functional mitochondria activity despite impaired mitophagy. These findings suggested that impaired mitophagy reduced, but did not totally abolish, adaptive thermogenesis during chronic cold exposure. Further studies using indirect calorimetry to compare *Atg*5 KO and *Ucp*1 KO mice under similar cold stress conditions would be useful for analyzing the degree of thermogenic impairment specifically due to loss of autophagy versus complete loss of *Ucp1*.

Chronic cold exposure increased short-, medium-, and long-chain acylcarnitines as well as increased *Cpt1a* and *Mcad* mRNA expression in BAT (Figure 2). These findings strongly suggested there was increased acylcarnitine flux and β-oxidation of fatty acids. Interestingly, pPNPLA2 and pLIPE also were down-regulated in BAT during chronic cold exposure (Figure 2E) suggesting that enzymatic hydrolysis of triglycerides was not a major mechanism for generating fatty acid substrates for β-oxidation. Our findings were consistent with a previous study that showed that acute cold exposure markedly stimulated BAT lipolysis to provide fuel for β-oxidation and generate heat, which then led to rapid depletion of lipid droplets after 12 h (Christoffolete et al., 2004). Moreover, lipophagy contributed to this process by breaking down lipid droplets stored in BAT (Martinez-Lopez et al., 2016; Zhang et al., 2020). Somewhat surprisingly, we did not observe autophagosomes-containing lipid droplets in the electron micrographs of BAT from mice chronically exposed to cold temperature (Figure 3A). It is possible that there was rapid lipophagy of fat droplets that was difficult to detect by electron microscopy or perhaps direct utilization of fatty acids generated by white adipose tissue lipolysis did not require incorporation into fat droplets after uptake by BAT during chronic cold exposure. However, it is noteworthy that phosphorylation of PRKAA and PNPLA2 were increased in BAT from

Atg5 KO mice after chronic cold exposure. Thus it appears that compensatory lipase activity was stimulated when autophagy (presumably lipophagy) was inhibited (Figure 4G).

Besides its effects on lipid metabolism and mitochondrial quality control during chronic cold stimulation, autophagy also may have effects on other cellular processes in BAT. Cold acclimation induced hyperplasia of BAT with significant proliferation of preadipocytes and vascular endothelial cells (Klingenspor, 2003; Bukowiecki et al., 1986; Fukano et al., 2016). In this connection, autophagy was found to regulate both brown adipocyte differentiation (Fu et al., 2019; Martinez-Lopez et al., 2013) and angiogenesis (Hassanpour et al., 2018; Du et al., 2012). Chronic cold exposure also induced the conversion of competent WAT into brown-like fat cells that have thermogenic potential (browning) (Herz and Kiefer, 2019; Wu et al., 2013; Lin et al., 2015). Further studies are needed to better understand the role of autophagy in these chronic processes induced by long-term cold exposure.

In summary, our study demonstrated that chronic cold exposure and/or NE stimulation induced autophagy, β-oxidation of fatty acids, and mitochondrial turnover and activity in BAT and primary brown adipocytes. Autophagy played a critical role in maintaining mitochondrial integrity and function that is necessary for thermogenesis during chronic cold exposure *in vivo*. Mitophagy was induced in BAT during chronic cold exposure, and its loss led to impaired thermogenesis *in vivo* and decreased respiration in primary brown adipocytes. BAT activity has been negatively associated with obesity and diabetes in man (Cypess and Kahn, 2010; Yoneshiro et al., 2019). Thus, our results support the notion that pharmacological modulation of autophagy in BAT to mimic the thermogenic effects observed during chronic cold exposure may be a potential approach to improve BAT activity for the treatment of metabolic diseases such as obesity and diabetes.

Limitations of the study

It is possible that chronic cold exposure has effects on BAT that are independent of sympathetic activation. However, we were unable to perform BAT denervation to examine cold-induced autophagy with impaired sympathetic nerve activation. It is also possible that lipophagy plays a role in facilitating fatty acid oxidation in chronic cold exposure to sustain thermogenesis. However we did not show evidence of lipophagy because this is beyond the scope of this study.

Resource availability

Lead contact

Further information and requests for resources and reagents should be directed to and will be fulfilled by the lead contact, Paul Michael Yen, MD (paul.yen@duke-nus.edu.sg).

Materials availability

This study did not generate new reagents. All reagents are commercially available.

Data and code availability

This study did not generate new dataset or code.

METHODS

All methods can be found in the accompanying Transparent methods supplemental file.

SUPPLEMENTAL INFORMATION

Supplemental information can be found online at https://doi.org/10.1016/j.isci.2021.102434.

ACKNOWLEDGMENTS

The research was funded by National Medical Research Council in Singapore (NMRC) (CSASI19may-0002) (P.M.Y.), NMRC/CIRG/1457/2016 (P.M.Y.), MOH-000319 (MOH-OFIRG19may-0002) (B.K.S.) and the Citrin Foundation (W.W.Y).

The author would like to thank Dr. Rohit A. Sinha, Dr. Madhulika Tripathi, Dr. Eveline Bruinstroop, Dr. Ronny Lesmana, Dr. Kenji Ohba, Mr. Sherwin Xie, Ms. Andrea Lim, Ms. Jiapei Ho, and Dr. Ufuk Degirmenci for their

helpful advice, technical support, and reagents. We are thankful to Prof. Jean-Paul Kovalik and Prof. Jianhong Ching for performing metabolic profiling (Metabolomics@ Duke-NUS). We would also like to thank Prof. T. Yoshimori (Osaka University, Osaka, Japan) and Dr. Andreas Till (Institute of Clinical Molecular Biology Christian-Albrechts-University of Kiel; Kiel, Germany) for gifting plasmids.

AUTHOR CONTRIBUTIONS

Conceptualization, W.W.Y., K.A.W., and P.M.Y.; methodology, W.W.Y., K.A.W., and P.M.Y.; investigation, K.A.W., W.W.Y., N.K.T., B.K.S., J.Z., and Y.W.; writing – original draft, K.A.W. and W.W.Y.; writing – review & editing, W.W.Y., K.A.W., B.K.S., and P.M.Y.; funding acquisition, P.M.Y. and B.K.S.; resources, B.-H.B. and P.M.Y.; supervision, P.M.Y.

DECLARATION OF INTERESTS

The authors declare no competing interests.

Received: June 22, 2020
Revised: February 11, 2021
Accepted: April 13, 2021
Published: May 21, 2021

REFERENCES

Barja De Quiroga, G., Lopez-Torres, M., Perez-Campo, R., Abelenda, M., Paz Nava, M., and Puerta, M.L. (1991). Effect of cold acclimation on GSH, antioxidant enzymes and lipid peroxidation in brown adipose tissue. Biochem. J. *277* (Pt 1), 289–292.

Bingol, B., and Sheng, M. (2016). Mechanisms of mitophagy: PINK1, parkin, USP30 and beyond. Free Radic. Biol. Med. *100*, 210–222.

Blondin, D.P., Daoud, A., Taylor, T., Tingelstad, H.C., Bezaire, V., Richard, D., Carpentier, A.C., Taylor, A.W., Harper, M.E., Aguer, C., and Haman, F. (2017). Four-week cold acclimation in adult humans shifts uncoupling thermogenesis from skeletal muscles to brown adipose tissue. J. Physiol. *595*, 2099–2113.

Blondin, D.P., Labbe, S.M., Tingelstad, H.C., Noll, C., Kunach, M., Phoenix, S., Guerin, B., Turcotte, E.E., Carpentier, A.C., Richard, D., and Haman, F. (2014). Increased brown adipose tissue oxidative capacity in cold-acclimated humans. J. Clin. Endocrinol. Metab. *99*, E438–E446.

Bukowiecki, L.J., Geloen, A., and Collet, A.J. (1986). Proliferation and differentiation of brown adipocytes from interstitial cells during cold acclimation. Am. J. Physiol. *250*, C880–C887.

Burman, J.L., Pickles, S., Wang, C., Sekine, S., Vargas, J.N.S., Zhang, Z., Youle, A.M., Nezich, C.L., Wu, X., Hammer, J.A., and Youle, R.J. (2017). Mitochondrial fission facilitates the selective mitophagy of protein aggregates. J. Cell Biol. *216*, 3231–3247.

Buzadzic, B., Korac, B., and Petrovic, V.M. (1999). The effect of adaptation to cold and re-adaptation to room temperature on the level of glutathione in rat tissues. J. Therm. Biol. *24*, 373–377.

Cairo, M., Villarroya, J., Cereijo, R., Campderros, L., Giralt, M., and Villarroya, F. (2016). Thermogenic activation represses autophagy in brown adipose tissue. Int. J. Obes. (Lond) *40*, 1591–1599.

Cannon, B., and Nedergaard, J. (2004). Brown adipose tissue: function and physiological significance. Physiol. Rev. *84*, 277–359.

Christoffolete, M.A., Linardi, C.C., De Jesus, L., Ebina, K.N., Carvalho, S.D., Ribeiro, M.O., Rabelo, R., Curcio, C., Martins, L., Kimura, E.T., and Bianco, A.C. (2004). Mice with targeted disruption of the Dio2 gene have cold-induced overexpression of the uncoupling protein 1 gene but fail to increase brown adipose tissue lipogenesis and adaptive thermogenesis. Diabetes *53*, 577–584.

Cypess, A.M., and Kahn, C.R. (2010). Brown fat as a therapy for obesity and diabetes. Curr. Opin. Endocrinol. Diabetes Obes. *17*, 143–149.

Du, J., Teng, R.J., Guan, T., Eis, A., Kaul, S., Konduri, G.G., and Shi, Y. (2012). Role of autophagy in angiogenesis in aortic endothelial cells. Am. J. Physiol. Cell Physiol. *302*, C383–C391.

Egan, D.F., Shackelford, D.B., Mihaylova, M.M., Gelino, S., Kohnz, R.A., Mair, W., Vasquez, D.S., Joshi, A., Gwinn, D.M., Taylor, R., et al. (2011). Phosphorylation of ULK1 (hATG1) by AMP-activated protein kinase connects energy sensing to mitophagy. Science *331*, 456–461.

Fu, X., Jin, L., Han, L., Yuan, Y., Mu, Q., Wang, H., Yang, J., Ning, G., Zhou, D., and Zhang, Z. (2019). miR-129-5p inhibits adipogenesis through autophagy and may Be a potential biomarker for obesity. Int. J. Endocrinol. *2019*, 5069578.

Fukano, K., Okamatsu-Ogura, Y., Tsubota, A., Nio-Kobayashi, J., and Kimura, K. (2016). Cold exposure induces proliferation of mature Brown adipocyte in a ss3-adrenergic receptor-mediated pathway. PLoS One *11*, e0166579.

Gospodarska, E., Nowialis, P., and Kozak, L.P. (2015). Mitochondrial turnover: a phenotype distinguishing brown adipocytes from interscapular brown adipose tissue and white adipose tissue. J. Biol. Chem. *290*, 8243–8255.

Hassanpour, M., Rezabakhsh, A., Pezeshkian, M., Rahbarghazi, R., and Nouri, M. (2018). Distinct role of autophagy on angiogenesis: highlights on the effect of autophagy in endothelial lineage and progenitor cells. Stem Cell Res. Ther. *9*, 305.

Herz, C.T., and Kiefer, F.W. (2019). Adipose tissue browning in mice and humans. J. Endocrinol. *241*, R97–R109.

Hinchy, E.C., Gruszczyk, A.V., Willows, R., Navaratnam, N., Hall, A.R., Bates, G., Bright, T.P., Krieg, T., Carling, D., and Murphy, M.P. (2018). Mitochondria-derived ROS activate AMP-activated protein kinase (AMPK) indirectly. J. Biol. Chem. *293*, 17208–17217.

Jin, S.M., and Youle, R.J. (2012). PINK1- and Parkin-mediated mitophagy at a glance. J. Cell Sci. *125*, 795–799.

Kim, Y.C., and Guan, K.L. (2015). mTOR: a pharmacologic target for autophagy regulation. J. Clin. Invest. *125*, 25–32.

Klingenspor, M. (2003). Cold-induced recruitment of brown adipose tissue thermogenesis. Exp. Physiol. *88*, 141–148.

Laker, R.C., Xu, P., Ryall, K.A., Sujkowski, A., Kenwood, B.M., Chain, K.H., Zhang, M., Royal, M.A., Hoehn, K.L., Driscoll, M., et al. (2014). A novel MitoTimer reporter gene for mitochondrial content, structure, stress, and damage in vivo. J. Biol. Chem. *289*, 12005–12015.

Lettieri-Barbato, D. (2019). Redox control of non-shivering thermogenesis. Mol. Metab. *25*, 11–19.

Lin, J.Z., Martagon, A.J., Cimini, S.L., Gonzalez, D.D., Tinkey, D.W., Biter, A., Baxter, J.D., Webb, P., Gustafsson, J.A., Hartig, S.M., and Phillips, K.J. (2015). Pharmacological activation of thyroid hormone receptors elicits a functional conversion of white to Brown fat. Cell Rep. *13*, 1528–1537.

Lowell, B.B., and Spiegelman, B.M. (2000). Towards a molecular understanding of adaptive thermogenesis. Nature *404*, 652–660.

Lu, Y., Fujioka, H., Joshi, D., Li, Q., Sangwung, P., Hsieh, P., Zhu, J., Torio, J., Sweet, D., Wang, L., et al. (2018). Mitophagy is required for brown adipose tissue mitochondrial homeostasis during cold challenge. Sci. Rep. *8*, 8251.

Mao, K., and Klionsky, D.J. (2011). AMPK activates autophagy by phosphorylating ULK1. Circ. Res. *108*, 787–788.

Martinez-Lopez, N., Athonvarangkul, D., Sahu, S., Coletto, L., Zong, H., Bastie, C.C., Pessin, J.E., Schwartz, G.J., and Singh, R. (2013). Autophagy in Myf5+ progenitors regulates energy and glucose homeostasis through control of brown fat and skeletal muscle development. EMBO Rep. *14*, 795–803.

Martinez-Lopez, N., Garcia-Macia, M., Sahu, S., Athonvarangkul, D., Liebling, E., Merlo, P., Cecconi, F., Schwartz, G.J., and Singh, R. (2016). Autophagy in the CNS and periphery coordinate lipophagy and lipolysis in the Brown adipose tissue and liver. Cell Metab. *23*, 113–127.

Meyer, C.W., Willershauser, M., Jastroch, M., Rourke, B.C., Fromme, T., Oelkrug, R., Heldmaier, G., and Klingenspor, M. (2010). Adaptive thermogenesis and thermal conductance in wild-type and UCP1-KO mice. Am. J. Physiol. Regul. Integr. Comp. Physiol. *299*, R1396–R1406.

Murholm, M., Dixen, K., Qvortrup, K., Hansen, L.H., Amri, E.Z., Madsen, L., Barbatelli, G., Quistorff, B., and Hansen, J.B. (2009). Dynamic regulation of genes involved in mitochondrial DNA replication and transcription during mouse brown fat cell differentiation and recruitment. PLoS One *4*, e8458.

Rabinovitch, R.C., Samborska, B., Faubert, B., Ma, E.H., Gravel, S.P., Andrzejewski, S., Raissi, T.C., Pause, A., St-Pierre, J., and Jones, R.G. (2017). AMPK maintains cellular metabolic homeostasis through regulation of mitochondrial reactive oxygen species. Cell Rep. *21*, 1–9.

Shabalina, I.G., Hoeks, J., Kramarova, T.V., Schrauwen, P., Cannon, B., and Nedergaard, J. (2010). Cold tolerance of UCP1-ablated mice: a skeletal muscle mitochondria switch toward lipid oxidation with marked UCP3 up-regulation not associated with increased basal, fatty acid- or ROS-induced uncoupling or enhanced GDP effects. Biochim. Biophys. Acta *1797*, 968–980.

Silva, J.E. (2003). The thermogenic effect of thyroid hormone and its clinical implications. Ann. Intern. Med. *139*, 205–213.

Stock, M.J. (1989). Thermogenesis and brown fat: relevance to human obesity. Infusionstherapie *16*, 282–284.

Sukumaran, A., Choi, K., and Dasgupta, B. (2020). Insight on transcriptional regulation of the energy sensing AMPK and biosynthetic mTOR pathway genes. Front. Cell Dev. Biol. *8*, 671.

Terskikh, A., Fradkov, A., Ermakova, G., Zaraisky, A., Tan, P., Kajava, A.V., Zhao, X., Lukyanov, S., Matz, M., Kim, S., et al. (2000). "Fluorescent timer": protein that changes color with time. Science *290*, 1585–1588.

Wei, H., Liu, L., and Chen, Q. (2015). Selective removal of mitochondria via mitophagy: distinct pathways for different mitochondrial stresses. Biochim. Biophys. Acta *1853*, 2784–2790.

Wu, J., Cohen, P., and Spiegelman, B.M. (2013). Adaptive thermogenesis in adipocytes: is beige the new brown? Genes Dev. *27*, 234–250.

Yau, W.W., Singh, B.K., Lesmana, R., Zhou, J., Sinha, R.A., Wong, K.A., Wu, Y., Bay, B.H., Sugii, S., Sun, L., and Yen, P.M. (2019). Thyroid hormone (T3) stimulates brown adipose tissue activation via mitochondrial biogenesis and MTOR-mediated mitophagy. Autophagy *15*, 131–150.

Yoneshiro, T., Wang, Q., Tajima, K., Matsushita, M., Maki, H., Igarashi, K., Dai, Z., White, P.J., Mcgarrah, R.W., Ilkayeva, O.R., et al. (2019). BCAA catabolism in brown fat controls energy homeostasis through SLC25A44. Nature *572*, 614–619.

Yu, J., Zhang, S., Cui, L., Wang, W., Na, H., Zhu, X., Li, L., Xu, G., Yang, F., Christian, M., and Liu, P. (2015). Lipid droplet remodeling and interaction with mitochondria in mouse brown adipose tissue during cold treatment. Biochim. Biophys. Acta *1853*, 918–928.

Zhang, X., Wu, D., Wang, C., Luo, Y., Ding, X., Yang, X., Silva, F., Arenas, S., Weaver, J.M., Mandell, M., et al. (2020). Sustained activation of autophagy suppresses adipocyte maturation via a lipolysis-dependent mechanism. Autophagy *16*, 1668–1682.

iScience, Volume *24*

Supplemental information

Chronic cold exposure induces autophagy to promote fatty acid oxidation, mitochondrial turnover, and thermogenesis in brown adipose tissue

Winifred W. Yau, Kiraely Adam Wong, Jin Zhou, Nivetha Kanakaram Thimmukonda, Yajun Wu, Boon-Huat Bay, Brijesh Kumar Singh, and Paul Michael Yen

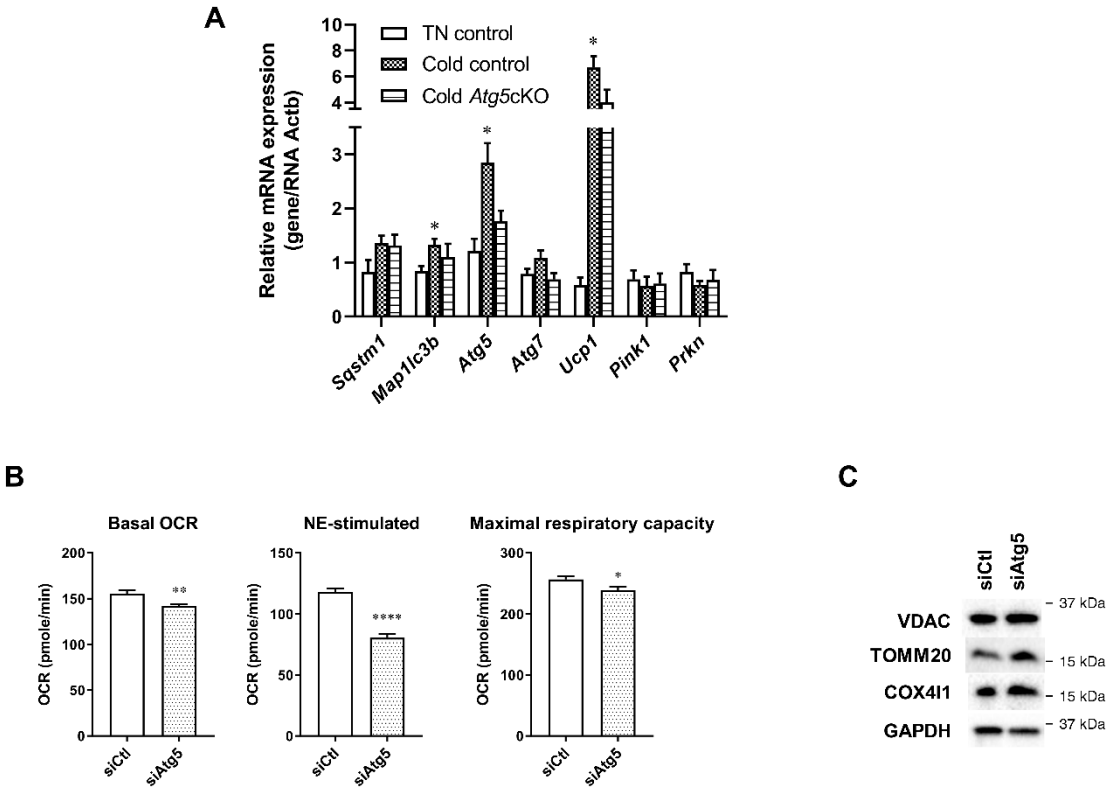

Figure S1. Autophagy in BAT is required for thermogenesis in chronic cold exposure, Related to Figure 4

(A) mRNA expression of autophagy gene in BAT of control and *Atg5*cKO mice housed at thermoneutral condition or in cold for 72 hours. Values are means±SEM for 5 mice in each group. (B) Basal, NE-stimulated and maximal OCR in primary brown adipocytes transfected with control or *Atg5* siRNA for 48 hr before analysis (C) Representative immunoblots and densitometry showing mitochondrial proteins in primary brown adipocytes transfected with control or *Atg5* siRNA for 48 hr. Statistical significance shows as *p<0.05, **p<0.01 and ****p<0.0001.

Transparent Methods

Study approval

All mice were maintained according to the Guide for the Care and Use of Laboratory Animals (NIH publication no. 1.0.0. Revised 2011), and experiments were approved by the IACUC at Duke-NUS Graduate Medical School.

Statistics

All cell culture related experiments were performed in triplicate and independently repeated to ensure data reproducibility. Data were pooled and represented as either mean ± SD for cell culture experiments or mean ± SEM for animal experiments.
Densitometry data were calculated for all Fig.s using ImageJ (Rasband, W.S., ImageJ, U.S. National Institutes of Health, Bethesda, Maryland, USA) were pooled and represented as mean ± SD. Statistical significance of differences ($p < 0.05$) was examined by two-tailed Student's t-test or one-way analysis of variance followed by Tukey post-hoc test using GraphPad PRISM v8.0 (GraphPad Software, Inc.).

Reagents

Unless otherwise specified, all chemicals were obtained from Sigma-Aldrich and all culture media were from Gibco (Thermo Fisher Scientific). Transfection reagents and siRNA (Ambion, 4390771) were purchased from Thermo Fisher Scientific. The tandem RFP/GFP-tagged LC3 plasmid and mito-RFP-EGFP plasmids were kind gifts from Prof. T. Yoshimori (Osaka University, Osaka, Japan) and Dr Andreas Till (Institute of Clinical Molecular Biology Christian-Albrechts-University of Kiel; Kiel, Germany), respectively. pMitoTimer was a gift from Zhen Yan (Addgene, 52659). Norepinephrine (NE) was purchased from Sigma-Aldrich (A0937).

Animals and experimental protocol

Male C57BL/6 mice (8 to 10 wk old) were housed in hanging polycarbonate cages and kept on a 12 h light-dark cycle in a temperature-controlled room at 24°C. They were allowed *ad libitum* access to water and a standard laboratory chow. Mice are house at thermoneutral condition (30°C) or in cold (4°C) for 72 hr before sacrifice. Animals were treated in accordance with the Guide for the Care and Use of Laboratory Animals and experiments were approved by the Institutional Animal Care and Use Committee (IACUC) and Duke-NUS Graduate Medical School. Body temperature was measured using a rectal probe after 72 hr exposure to thermoneutral condition (30°C) or cold (4°C).

Adenoviral infection

For tissue-specific knockout study, male homozygous *Atg5*$^{Flox/Flox}$ mice (C57BL/6/129) were obtained from the Riken BioResource Center, Japan, courtesy of Dr. Noboru Mizushima. A total of 5×10^{11} genome copies of control adenovirus or Ucp1-Cre-expressing adeno-associated virus (Vector BioLabs, AAV8-UCP1-eGFP and AAV8-UCP1-iCre) was injected into tail vein of 8-week-old male *Atg5*$^{Flox/Flox}$ mice for four weeks before initiating the cold exposure experiments. Core body temperature was measured using a rectal temperature probe on the last day of cold challenge.

Primary culture of brown preadipocytes

Primary brown adipocytes were derived from the interscapular BAT of 2 to 3 weeks old C57BL/6 mice. The precursor cells were isolated according to the protocols described by Rehnmark et al. and Klein et al. Briefly, BAT from 6 to 8 mice was cut into small pieces and digested with 0.2% (w:v) collagenase (Sigma-Aldrich, C6885) for 30 min in a shaking water

bath. After filtering through a 150-μm nylon screen (Fisher Scientific, 22363549), the pellet containing preadipocytes were collected by centrifugation at 200 g for 5 min. Preadipocytes were maintained in DMEM (Gibco, 11995–065) supplemented with 15% heat inactivated FBS (Gibco, 10500–064), non-essential amino acids (Gibco, 11140–076), 5 ng/ml human basic FGF (Thermo Fisher Scientific, PHG0021), 100 U/ml penicillin and 50 μg/ml streptomycin (Sigma-Aldrich, F7524). Differentiation was initiated with DMEM containing 10% fetal bovine serum (FBS; Gibco, 15140122), dexamethasone (Sigma-Aldrich, D1756), 3-isobutyl-1-methylxanthine (IBMX) (Sigma-Aldrich, I5879) and insulin (Sigma-Aldrich, I9278). Cells were allowed to differentiate for 6 d before treatment. For NE treatment, cells were treated with 1 μM NE for 0, 6, 24 or 72 hr. For autophagic flux assay, cells were treated with 50 nM bafilomycin A1/Baf (Sigma-Aldrich, B1793) 6 hr before harvest. For RNA interference studies, Lipofectamine® RNAiMAX Reagent (Invitrogen, 13778075) was used to transfect the cells 48 hr before NE treatment.

Cell line transfection

Plasmid transfection were performed in the brown adipocyte cell line mBAP-9 (Wu and Smas, 2008). Cells were seeded on cell culture slide (SPL Life Sciences, 30104) and maintained in DMEM containing 10% FBS and differentiated by DMEM containing 10% FBS, insulin, T_3, dexamethasone and IBMX for 6 d before treatment. Transfection was carried out 2 d before treatment using Lipofectamine® 3000 Reagent (Invitrogen, L3000008) in accordance to the manufacturer's protocols. After transfection, cells were treated with 1 μM of NE for 72 h before fixation with 4% paraformaldehyde (Sigma-Aldrich, P6148). Cell imaging was performed using a Zeiss LSM 710 Confocal Microscope.

Protein carbonylation

The amount of protein carbonyls was measured with an OxyBlot™ Oxidized Protein Detection Kit (EMD Millipore, S7150) according to the manufacturer's protocol.

RNA isolation and quantitative reverse transcription polymerase chain reaction

Total RNA was extracted from the BAT with TRIzol reagent (Invitrogen) followed by InviTrap spin cell RNA Minikit (Stratec Molecular) according to the manufacturer's instructions. RNA concentration was measured by NanoDrop 8000 (Thermo Scientific), and cDNA was reverse transcribed from 1000 ng of total RNA using high-capacity cDNA reverse transcription kits (BioRad). The quantitative reverse transcription polymerase chain reactions (qRT-PCRs) were performed using the QuantiFast SYBR Green PCR Kit (QIAGEN) on the 7900HT Fast Real-Time PCR system (Applied Biosystems). Relative mRNA levels were calculated using the $2^{-\Delta\Delta Ct}$ method and normalized to suitable reference genes following cold exposure. Data are expressed as the fold change relative to the mean value of non-treated mice.

Electron microscopy

Cells were seeded in a 4-chambered coverglass (Thermo Scientific Nunc, NNU 155383-PK) and allowed to differentiate for 7 d before addition of NE or bafilomycin A1 (Baf; Sigma-Aldrich, B1793). After treatment, cells were fixed with 2.5% glutaraldehyde (nacalai tesque, 17025–25) in sodium phosphate buffer (0.1 M, pH 7.4) and washed 3 times with phosphate buffered saline (PBS; Axil Scientific, BUF-2040-1X1L). The samples were then post-fixed with 1% osmium tetroxide and dehydrated with a series of alcohol with increasing concentration. After embedding samples in Araldite (Pelco, 18060), ultra-thin sections were cut and double-stained with uranyl acetate and lead citrate. Images were taken using the JEOL JEM-1010 transmission electron microscope (Japan).

Western blot analysis
Cells and tissues were dissociated in RIPA buffer (50 mM Tris-HCl, pH 8.0, 150 mM sodium chloride, 1% Triton X-100 (Bio-Rad, 1610407), 0.5% sodium deoxycholate (Sigma-Aldrich, D6750), 0.1% sodium dodecyl sulfate, 2 mM EGTA, 2 mM EDTA, protease inhibitors (Sigma-Aldrich, P8340) and phosphatase inhibitors (Sigma-Aldrich, P5726, P0044). Proteins were denatured by boiling in Laemmli sample buffer (250 mM Tris-HCl, pH 7.4, 2% w:v sodium dodecyl sulfate, 25% v:v glycerol, 50 mM DTT, 0.01% w:v bromophenol blue). Equal amount of proteins was resolved on sodium dodecyl sulfate-polyacrylamide gels using the Mini-PROTEAN 3 Electrophoresis unit and transferred to polyvinylidene difluoride membranes (Bio-Rad) using the TransBlot® Turbo™ Transfer System (Bio-Rad). The following antibodies were used to detect the target proteins. Cell Signaling Technology: MAP1LC3B (2775; RRID:AB_915950), SQSTM1 (5114; RRID:AB_10624872), COX4I1 (4850; RRID:AB_2085424), ATG5 (2630; RRID:AB_2062340), PRKAA (5831; RRID:AB_10622186), phospho-PRKAA (Thr172) (2535; RRID:AB_331250), ULK1 (8054; RRID:AB_11178668), phospho-ULK1 (S555) (5869; RRID:AB_10707365), MTOR (2983; RRID:AB_2105622), phospho-MTOR (Ser2448) (5536; RRID:AB_10691552), RPS6KB1 (9202; RRID:AB_331676), phospho-RPS6KB1 (T389) (9205; RRID:AB_330944), EIF4EBP1 (9452; RRID:AB_331692), phospho-EIF4EBP1 (Thr37/46) (2855; RRID:AB_560835), LIPE (4126; RRID:AB_490997), VDAC (4661; RRID:AB_10557420), DNM1L (8570; RRID:AB_10950498) and GAPDH (2118; RRID:AB_561053). Santa Cruz Biotechnology: TOMM20 (sc-11415; RRID:AB_2207533) and Abcam: UCP1 (ab10983; RRID:AB_2241462), phospho-PNPLA2 (S406) (ab135093; RRID:AB_2888660), PPARGC1A (ab191838; RRID:AB_2721267) and CPT1A (ab128568; RRID:AB_1114163).

Seahorse XF analyzer measurement for mitochondrial oxygen consumption rate (OCR)
Preadipocytes were seeded on XF-24-well culture microplates and allowed to differentiate for 7 d. After treatment, oxygen consumption was measured using a microplate (type XF24) extracellular analyzer (Seahorse Bioscience, Billerica, MA, USA). Reagents were optimized using the Mito stress kit from Seahorse Bioscience (Agilent, 100850–001) using the protocol and algorithm program in the analyzer. Oligomycin (1 μM), which inhibits the F0 proton channel of the F0F1-ATP synthase, was employed to determine the oligomycin-independent leak of the OCR. The mitochondrial uncoupler carbonyl cyanide 4-(trifluoromethoxy)phenylhydrazone (FCCP; 2 μM) was added to determine the total respiratory capacity of the mitochondrial electron transport chain. Rotenone (1 μM) and antimycin A (1 μM) (R+A) was added to block complex I and complex III of electron transport chain. The following mitochondrial functional parameters were calculated as follows: (i) basal O2 consumption = baseline OCR reading per well, before compounds are injected subtracting non-mitochondrial respiration (after R+A injection); (ii) NE stimulated = OCR reading per well after NE injection subtracting baseline OCR reading per well (before compounds are injected); (iii) maximum respiratory capacity = oxygen consumption reading per well (after FCCP injection) subtracting non-mitochondrial respiration (after R+A injection). Computed data were plotted as bar graphs.

Metabolic profiling of acylcarnitines
Acylcarnitines in BAT were measure in the Duke-NUS Metabolomics Facility according to previously established mass spectrometry (MS)-based methods. Briefly, brown adipose tissue was homogenized in 50% acetonitrile and 0.3% formic acid. For acylcarnitine extraction, 100 μl of tissue homogenate was extracted using methanol. The acylcarnitine extracts were derivatized with 3 M hydrochloric acid in methanol, dried, and reconstituted in methanol for analysis in liquid chromatography/mass spectrometry (LC/MS). Acylcarnitine measurements were made using flow injection–tandem mass spectrometry on the Agilent 6430 Triple

Quadrupole LC/MS system (Agilent Technologies, CA, USA). The sample analysis was carried out at 0.4 ml/min of 80:20 methanol:water as mobile phase and injection of 2 µl of sample. Data acquisition and analysis were performed on Agilent MassHunter Workstation B.06.00 software.